HHS Public Access

Author manuscript

Biomaterials. Author manuscript; available in PMC 2017 December 01.

Published in final edited form as:

Biomaterials. 2016 December ; 110: 24–33. doi:10.1016/j.biomaterials.2016.09.014.

Regenerated silk materials for functionalized silk orthopedic devices by mimicking natural processing

Chunmei Li[a], **Blake Hotz**[a], **Shengjie Ling**[a,b], **Jin Guo**[a], **Dylan S. Haas**[a], **Benedetto Marelli**[a,b], **Fiorenzo Omenetto**[a], **Samuel J. Lin**[c], and **David L. Kaplan**[a]

David L. Kaplan: david.kaplan@tufts.edu

[a]Department of Biomedical Engineering, Tufts University, 4 Colby St. Medford, MA 02155 USA

[b]Department of Civil and Environmental Engineering, Massachusetts Institute of Technology, 77 Massachusetts Avenue Cambridge, Massachusetts 02139 USA

[c]Divisions of Plastic Surgery and Otolaryngology, Beth Israel Deaconess Medical Center, Harvard Medical School, Boston, Massachusetts 02215 USA

Abstract

Silk fibers spun by silkworms and spiders exhibit exceptional mechanical properties with a unique combination of strength, extensibility and toughness. In contrast, the mechanical properties of regenerated silk materials can be tuned through control of the fabrication process. Here we introduce a biomimetic, all-aqueous process, to obtain bulk regenerated silk-based materials for the fabrication of functionalized orthopedic devices. The silk materials generated in the process replicate the nano-scale structure of natural silk fibers and possess excellent mechanical properties. The biomimetic materials demonstrated excellent machinability, providing a path towards the fabrication of a new family of resorbable orthopedic devices where organic solvents are avoided, thus allowing functionalization with bioactive molecules to promote bone remodeling and integration.

Keywords

silk; biomimetic; self assembly; orthopedic

1. Introduction

The outstanding mechanical properties of natural silk fibers derive from their unique structure, which is determined by spinning process and the nature of the spinning solution. In the natural spinning process of silkworm, *Bombyx mori*, the silk fibroin (hereafter referred to as silk) concentration increases gradually and controllably from ~12% to 30% as the silk molecules move from the posterior to the anterior region of the silk glands [1].

*Corresponding author: david.kaplan@tufts.edu, Fax: 617-627-3231.

Meanwhile, the chains assemble to micelles, follow by arrange and stack them together in a step-by-step manner, and form the compact solid architecture under regulation of external environments, such as pH, ion concentration, physical shear and/or elongational flow [2]. Many efforts have been explored to regenerate silk materials with mechanical properties comparable to or exceeding those of natural silk fibers [3–5]. Silk fibers stronger and tougher than natural undegummed *B. mori* silkworm silk have been obtained from regenerated *B. mori* silk solutions *via* microfluidic chip [3] and wet spinning [5]. One common feature of those studies is a spinning dope of highly concentrated silk solutions, which is a prerequisite to form a dense, compact solid structure in natural spinning process [1]. However, the focus has mainly been limited to the generation one-dimensional silk fibers in the micrometer range, which significantly hinders their application. There is need to develop three-dimensional silk materials in larger dimensions that can be used to fabricate devices with high mechanical demands, such as orthopedic devices.

Metals like titanium alloys and stainless steel remain the gold standard for orthopedic devices due to their robust mechanical properties and ease of fabrication and implantation, whereas limitations of stress shielding, infections, bone remodeling and second surgical removal have shifted significant interest to degradable devices [6, 7]. Resorbable orthopedic devices composed of poly-L-lactic acid and polyglycolic acid reduces the need for hardware removal and improved bone remodeling. However, the degradation of these resorbable devices is associated with inflammatory foreign body reactions due to the acidic degradation products, osteolysis and incomplete bone remodeling [8]. In addition, orthopedic devices are historically designed to provide mechanical stability to the surrounding bone and soft tissue, whereas functionalization of the device to improve the implant integration and mitigate adverse events associated with the foreign body reaction or infection has been largely neglected [8]. Only recently, a few functionalization methods have been developed *via* applying biological coating to orthopedic devices to modulate the surrounding microenvironment. These approaches inlclude coatings to enhance osteointegration (*e.g.*, calcium phosphate-like coatings [10–13] and biomolecules coatings [14–18] and coatings to mitigate foreign body reaction (*e.g.*, bisphsphonates coatings [19–21]) and infection (*e.g.*, adhesion resistant coating [22–24], coatings with antibiotics [25, 26] and silver impregnated coatings [27, 28]). Surface coatings normally involve complicated procedures and they do not always possess long-term stability due to the degradation and detachment of the coatings. In contrast, bulk-incorporated bioactive molecules can exert their effects *via* both surface contact and sustained release. However, the bulk incorporation of labile biomolecules in current orthopedic devices remains a challenge due to the harsh conditions of the manufacturing process. Therefore, degradable orthopedic devices with appropriate mechanical properties, pro-osteogenic and antimicrobial features, would have a major impact on orthopedic repairs in promoting accelerated healing, reducing second surgeries and improving long-term patient outcomes.

Silk is an unique candidate to address these issue due to its excellent mechanical properties, biocompatibility, tunable degradability [29, 30], as well as the ability of silk to stabilize various of bioactive compounds [31]. We recently demonstrated the feasibility of silk protein as a molding and machinable biomaterial system for the preparation of devices for craniofacial repairs, based on the use of an organic solvent-based process (1,1,1,3,3,3

hexafluro-2-propanol (HFIP)) [29]. To obtain water-stable structures, HFIP was required to facilitate silk solubility and methanol to induce the formation of β-sheet structure [29]. However, HFIP can limit utility due to cost, risk for residuals in the devices, and difficulty in incorporating labile biomolocules in the fabrication process. These caveats drive us to develop new types of silk orthopedic implants basing on the aqueous silk solution. However, high concentration aqueous silk solution (> 20%, wt/wt), a prerequisite to form a dense, compact solid structure in natural silk spinning process [1], is highly instable and shows a strong tendency to form hydrogels or aggregates, which introduces challenges and increases complexity throughout the fabrication process. Natural spinning process of spiders and silkworms have inspired us to build bulk silk materials in a more facile and "green" way. In the present study, we developed a biomimetic process to generate bulk silk materials that avoided the use of organic solvents and harsh chemicals. The regenerated silk materials have excellent machinability and were successfully machined into various orthopedic devices. Importantly, the mild aqueous-based process facilitates the bulk incorporation of dopants and bioactive compounds, thus providing additional clinical benefits like osteoinductive, osteoconductive and anti-microbial/anti-inflammatory features.

2. Materials and Methods

2.1. Preparation of aqueous silk solution

Silk fibroin solution was prepared from *B. mori* cocoons using our established protocol with some modifications [32]. First, sericin was removed by boiling the cocoon pieces in 0.02 M aqueous Na_2CO_3 solution for 30 minutes followed by extensive rinses in distilled water. The degummed silk was then dried overnight and dissolved in 9.3 M LiBr at 60°C for 4 hours, yielding a 20% (w/v) solution. The pH of LiBr solution was adjusted by adding 1 M LiOH solution so that the pH of the final silk solution after dialysis was 8.0. The silk/LiBr solution was dialyzed against distilled water for 2 days with 10 changes of water. The solution was centrifuged for 2 × 20 min at 9,000 rpm. The silk concentration was determined by evaporating water from a solution of known weight and weighing the remaining solid using an analytical balance.

2.2. P24 synthesis

The BMP-2-related peptide P24 (SKIPKASSVPTEL-SAISTLYLDDD) was synthesized by Tufts university core facility. The peptides were made on an ABI 431 Peptide Synthesizer using Fmoc chemistry and HBTU activation. The purity of the peptides was greater than 90%.

2.3 Preparation of silk-based blanks for machining

Silk solution of 6–8 % (wt/wt) was subjected to forced airflow and water was slowly removed at 10°C until the silk concentration reached 25–30%. The concentration of the solution was monitored by weighing the remaining solid after drying. Rectangular molds with water-permeable membranes were used to prepare silk blanks for machining. As an example, 3–12 ml Slide-A-Lyzer dialysis cassette (Thermo Fisher, USA) with inner chamber dimensions of 65mm × 28mm × 6.5mm was loaded with concentrated silk solution and placed into a refrigerated incubator with forced air flow at 10°C for 3 to 4 days. Water

evaporated through the porous water-permeable membrane from both sides of the cassette and resulted in solid silk materials. The materials were then left in a fume hood for 4 days followed by another 4 days in a 45°C oven to remove the remaining water. To produce silk-based composite materials, silica (20–200 nm, Sigma, USA) and hydroxyapatite (HAP) (200 nm, Sigma, USA) were first dispersed in water by sonication and mixed with silk fibroin solution to obtain a suspension with desired amount of silica or HAP. The same dehydration procedure as described above was conducted to obtain silk/SiO_2 and silk/HAP composite blanks. To produce antibiotic-containing silk materials, a suspension of ciprofloxacin·HCl in water was mixed with 26.5% (wt/wt) silk solution to a final ciprofloxacin content of 5% (wt/wt). The mixture was loaded into molds and dehydrated at 10°C for 3 days followed by room temperature drying in a fume hood for 2 weeks. Osteoinductive silk materials were obtained in a similar way except that BMP-2 (Wyeth, USA) and P24 solution was mixed with concentrated silk solution at a concentration of 30 μg BMP2/g silk and 1.0 mg P24/g silk, respectively. The pH of silk solution used for BMP2 mixing was maintained at 6.5 to prevent the aggregation of BMP2 at pH 8, as BMP2 has an isoelectric point of 8.5 [15].

2.4. Machining of silk orthopedic devices

The silk blanks were machined into screws and intramedullary (IM) nails using a CNC lathe (Trak TRL 1440 EX). For IM nails, the silk blank was left on the CNC lather once the desired diameter was reached and a needle type tip was placed on the end for insertion. For screws with bone screw threads, a custom single point external cutter (Vargus, USA) was used on the CNC lathe to cut screw threads by matching turning speed with horizontal speed of the cutter to cut a desired pitch length (outer diameter ~ 1.8 mm, pitch = 600 μm). The screw heads were machined to have a cylindrical heads by use of the CNC lathe. Once machined, the screw or IM nail was then cut off behind the head or length of nail. A diamond cutter was mounted to the lathe and used to cut a slot in the screw head for screw insertion. For plates, rectangular silk blanks were machined using a CNC milling machine (Trak DPM). The milling machine was used to cut the desired shape of the mold and thickness (Figure S6). Once the plate was shaped and sized, cylindrical or conical screw holes were cut using a 90 degree Ford countersink.

2.5. Characterization

The morphology of the biomimetic silk materials and silk-based orthopedic devices were characterized by scanning electron microscopy (SEM) and atomic force microcopy (AFM). The structure was analysed with a JASCO 6200 FTIR spectrometer.

SEM: For morphological analysis, samples were sputtered coated with platinum and imaged with a Zeiss Supra55VP SEM (Cal Zeiss, Germany). Silk rod of 1.5 mm was fractured in liquid nitrogen and fracture surface was imaged under SEM.

AFM: AFM was performed on a MFP-3D-BIO AFM (Asylum Research, USA) with tapping mode. Cr/Au(5/45) coated silicon cantilever with a tip radius below 10 nm was used (k = 2 N/m, v ~ 70 kHz, Asylum Research, USA).

ATR–FTIR: SF solution of 26.5% was flash frozen in liquid nitrogen and freeze dried to preserve original structure before FTIR analysis. FTIR spectra were gathered utilizing FT/IR-6200 Spectrometer (Jasco, USA), equipped with a triglycine sulfate detector in attenuated total reflection (ATR) mode. The measurements were taken in the range of 4000–400 cm^{-1} at a resolution of 2 cm^{-1} with 128 scans. The background spectra were collected under the same conditions and subtracted from the scan for each sample.

2.6. Mechanical Testing

Mechanical characterization of the compressive properties of the silk and silk/HAP blanks were tested on an Instron 3366 (Instron, USA) testing frame equipped with a 10 kN load cell. Silk and silk/HAP blanks were machined into cylinders of 4 mm in diameter and 4 mm in height. All tests were performed using a displacement control mode at a rate of 5 mm/min.

The double lap shear test was performed on silk and silk/HAP (80/20, wt/wt) pins (1.5 mm in diameter and 6 mm in length) at dry state and hydrated environments by immersion in Dulbecco's PBS (ThermoFisher, USA) at 37 °C for 14 days. The fixture consists of three adjacent stainless steel plates with aligned holes of 1.5 mm that allow the tight fitting of the silk pins (Figure S7a). The bottom fixture remained stationary and the top fixture was mounted to an Instron 3366 test frame and compressed at a rate of 5 mm/min until fracture of the pins (ASTM standard F2502-11). Maximum shear stress was determined from the maximum load and the cross section area of the pins.

Silk plates with a width of 7 mm, length of 29 mm and thickness of 2 mm were tested for bending strength (Figure S6) at dry state. The plates were four-hole plates with 2 mm diameter holes. Holes were placed 3.5 mm from the ends of the plates with the nearest hole separated by 4.5 mm. The 2 center holes were separated by 13 mm. A four-point bending fixture was machined from stainless steel with brass loading rollers and support rollers (Figure S6b, supporting information), allowing rolling during testing to avoid frictional forces. The fixture has a loading span and center span of 6 mm with support rollers placed directly between the 2 outer holes. The bottom fixture remained stationary while the top fixture was mounted to an Instron 3366 test frame and compressed at a rate of 5 mm/min until fracture or complete compression to the bottom fixture. The bending stiffness, bending structural stiffness and bending strength were determined from the load *vs.* load-point displacement curve using the methods described in ASTM standard F2502-11. Bending modulus was determined using equation 1 [32].

$$E_{4p} = \frac{m_{4p} L_0^3}{8wt^3} \quad (1)$$

Where:

E_{4p} = 4-point bending modulus (MPa)

M_{4p} = 4-point bending stiffness (N/mm)

L_0 = length between support rollers (mm)

t = thickness of plate (mm)

w = width of plate (mm)

2.7. In vitro zone of inhibition test and antibiotics release

In vitro antibacterial effect of the ciprofloxacin-loaded silk orthopedic device was estimated by using the Kirby-Bauer susceptibility test. Briefly, 50 μl of the *Sraphylococcus aureus* (*S. aureus*, ATCC 25923) overnight culture ($[O.D]_{600nm}$ = 0.8–1.0) were plated on Tryptic Soy Agar plates. After 24 hours, the zone of inhibition was measured using image J software. Ciprofloxacin-containing silk pins (1.5 mm in diameter and 3–4 mm in length) were placed on the plates and incubated at 37 °C to allow bacteria to grow. The cirprofloxacin release was determined by immersing drug-loaded silk pins (5% wt/wt) in Dulbecco's PBS (0.2 mL) and PBS supplemented with protease IXV (5 unit/mL) at 37°C. At desired time points, the buffer was removed and replaced with fresh buffer. The amount of release was determined using the direct zone of inhibition assay. The active antibiotic was quantified by comparing zone of clearance in bacteria lawns with zones of clearance generated by standards of known antibiotic concentration..

2.8. Biofilm inhibition test

The ability of silk material functionalized with ciprofloxacin to inhibit development of biofilm on its surface was evaluated using *Sraphylococcus epidermidis* (*S. epidermidis,* ATCC 35989). Silk pins loaded with/without ciproprofloxacin (1.5mm in diameter, 3mm in length) were incubated in 4mL of a suspension of *S. epidermidis* ($[OD]_{600nm}$ = 0.2) in Trypticase Soy Broth (TSB) for 2 days. SEM was used to examine the biofilm formation. In brief, samples were fixed with 4% parafomaldehyde (PFA), followed by dehydration using a series of graded ethanol and dried by hexamethyldisilazane. The samples were then sputtered coated with platinum prior to SEM analysis.

2.9. Human mesenchymal stem cell (hMSCs) isolation and expansion

hMSCs were isolated from total bone marrow aspirate from a healthy, non-smoking male under the age of 25 (Lonza, USA). Whole bone marrow was diluted in expansion medium, plated in 175 cm^2 flasks (Corning, USA) at a density of 200,000 cells/cm^2 and cultured at 37 °C with 5% CO_2 in a humidified environment. Expansion media consisted of Dulbecco's modified eagle medium (DMEM), 10% fetal bovine serum (FBS), 1% non-essential amino acids, 1 ng/ml bFGF, and 1% antibiotic/antimycotic (ThermoFisher Scientific, NY, USA). Each flask contained a final volume of 35 ml, which was rocked daily to allow hemopoietic cells to remain in suspension and the stromal cells to adhere to the flask. The adherent cells were allowed to reach 80% confluence, after which they were trypsinized, suspended in FBS containing 10% DMSO and stored in liquid nitrogen. Second passage cells were used for experiments.

2.10. Osteogenic differentiation of hMSCs induced by BMP2/P24-incorporatd screws

Silk sponge of pore size of 400–500 μm was prepared as previously described [31]. Tubular silk sponge (2 mm inner diameter, 4 mm outer diameter, 4 mm height) were cut from the

sponge with dermal punches. Ethylene oxide sterilized BMP2- and P24-loaded silk screws were then inserted into the tubular sponge and one million hMSCs were seeded in the sponge. The construct was then maintained in osteogenic medium for 6 weeks. The harvested constructs were cut in half along the longitudinal axis in order to expose the interface of the screw and sponge. The samples were then stained with OsteoImage and observed under Keyence BZ-X710 fluorescent microscope.

2.11. Statistic analysis

Statistical analysis was performed by two-tailed Student's t-test using GraphPad software (GraphPad Prism software, CA). p values < 0.05 were considered statistically significant.

3. Results and Discussion

3.1 Regenerated silk materials by mimicking natural processing

Inspired by the natural spinning process (Figure 1a), we developed a "green", controllable strategy to create silk materials with unique structure that mimics the natural silk fibers (Figure 1b). Aqueous silk solution of 25–30%, matching the silk concentration in the anterior region of silkworm gland, was first obtained by a slow dehydration process. Highly concentrated aqueous silk solution (> 20% wt/wt) is highly instable and shows a strong tendency to form hydrogels or aggregates. Therefore, the pH of the silk solution was controlled at 8.0 and low temperature (10 °C) was maintained during dehydration to prevent early hydrogel formation. The concentrated silk solution was then loaded into molds to allow further water removal at 10°C without premature gelation. The remaining water was then removed by further dehydration at elevated temperatures, resulting in optically clear, solid silk blanks.

A remarkable feature of the silk blanks is their machinability. The silk blanks can be machined into various types of orthopedic devices, such as bone screws, plates and IM nails, which is discussed in detail in section 3.2. In comparison to our previously developed solvent-based system, the advent of an aqueous silk formulation to generate orthopedic devices with improved mechanical properties eliminates the risks with the use of toxic organic solvents. Furthermore, the mild aqueous-based process facilitates the addition of dopants and bioactive compounds during blank preparation, thus providing additional clinical benefits like osteoinductive, osteoconductive and anti-microbial/anti-inflammatory features. As illustrated in Figure 1c, silk blanks can also be machined into other desired shapes readily, such as cylinder, triangular prism, star and flash sign. Therefore, this new, bio-friendly silk biomimetic material may find use in the fabrication of engineered components with complex shapes and desired functionalities.

Structural insight into the self-assembled biomimetic materials was obtained by scanning electron microscopy (SEM) and atomic force microscopy (AFM). The combination of the two techniques revealed a uniform and dense structure composed of silk globules of around 30 nm in size (Figure 1d, e and f), reminiscent of the globular structure of the native silk fiber. Spider silk showed isotropic ~10 nm globules, whereas silkworm silk generates globules that are anistropic ~23nm ×16 nm [35]. Another unique feature of the regenerated

silk materials is the hierarchical organization of the material. Silk nano-globules formed aggregates of tens to hundreds of nanometer in size (Figure 1e, white circle), and these aggregates interacted with each other to form a dense network. The density of the biomimetic silk materials was estimated to be 1.39 ± 0.04 $g \cdot cm^{-3}$ based on the mass and volume of machined cylindrical samples (1.5 mm in diameter and 5 mm in length), which is comparable to that of the native silk. This result is in line with the microstructural resemblance between the biomimetic silk materials and natural silk fiber.

Fourier transform infrared spectroscopy (FTIR) was used to monitor the structural change during the assembly process of the silk materials (Figure 1g). The 1515 cm^{-1} band in amide II region, assigned to the aromatic ring C-C stretching of the tyrosine (Tyr) side chain, is a local monitor for the conformational change and hydrophilicity of the Tyr microenvironment [36]. A decrease in the wavenumber to 1512 cm^{-1} was observed with dehydration, which could be related to a more hydrophobic microenvironment induced by peptide folding [37]. After dehydration at 10°C for 3 days and room temperature for 4 days, absorbance bands appeared around 1632 and 1697 cm^{-1} (plot B in Figure 1g), indicating the formation of intramolecular and intermolecular β-sheet structure, respectively [38]. Further dehydration at 45°C did not induce significant changes in silk structure (plot C in Figure 1g).

Figure 1j sketched the structural evolution of silk molecules in our designed biomimetic fabrication process, according to the aforementioned structural evidences. Protein molecules tend to further form reversible cluster/aggregates due to the contribution of attractive forces and repulsive excluded volume effect [39–41]. The silk molecules are present as oligomeric aggregates in concentrated silk solutions adopting mainly random coil structure (plot A in Figure 1g), similar to the silk molecules in spinning duct. As the local protein concentration increases with further dehydration, crystal nucleation between protein chains is trigged, leading to the formation of ordered fibrous/globular intermediate structures, consisting of nanosized globules. While water molecules continue to leave the system, these intermediate structures formed a network *via* hydrogen bonds and eventually a densely-packed solid silk material. The control of solution pH and slow dehydration process allows sufficient time for the fibroin chains to self assemble and thus β-sheet content increases over time (Figure 1g). The resulting materials exhibit a microstructure composed of interlocked nano-globules (Figure 1f), which is also the fundamental structures of nanofibrils in natural silk fiber [35]. These nano-globules of different sizes, which are responsible for the nonslip kinematics, restricted shearing between fibrils, allowing controlled local slipping and energy dissipation without bulk fracturing [42].

Considering the highly structural similarity with natural silks as well as superb mechanical performance of natural silk fibers, we sought to evaluate the mechanical properties of the biomimetic silk materials (Figure 1h). The compressive stress-strain profile was similar to that of natural bone: an elastic region followed by a plastic deformation phase. The compressive yield strength of 123.6 ± 8.6 MPa and modulus of 4.2 ± 0.4 GPa were well above the mechanical tolerance of cancellous bone (2–12 MPa and 50–500 MPa, respectively [43]) and approached that of cortical bone (100–230 MPa and 7–30 GPa, respectively [43]). Remarkably, the mechanical properties of biomimetic silk materials can be further improved by adding inorganic fillers. For example, when 20% nano-HAP, a

natural component of bone, was included in the silk materials, the compressive yield strength and modulus increased to 164.0 ± 5.9 MPa and 6.4 ± 0.7 GPa, respectively. In figure 1i, our biomimetic silk materials (yellow eclipse) are compared with the specific strength as a function of specific Young's modulus for natural silk fibers, bone and bone-substitute materials. The specific strength and modulus of the biomimetic silk materials were obtained from the stress-strain curves with a density of 1.39 ± 0.04 g·cm^{-3}. The specific modulus of the biomimetic silk materials is significantly higher than that of the cancellous bone, while comparable to the natural silk fibers and compact bone. Notably, the specific strength of the biomimetic silk materials is significantly higher than that of the dense polymer materials, while the specific modulus falls within the higher end values for dense polymer materials.

3.2 Silk orthopedic devices from biomimetic regenerated silk materials

In order to meet the morphology and structure requirements of orthopedic devices, we explored the machinability of the regenerated silk materials generated by the biomimetic aqueous process. Silk screws, pins and plates were successfully machined from silk blanks. The resultant silk screws (major diameter ~1.8 mm) appeared a glossy surface without any defects, and more importantly, showed distinct threads with sharp edges (Figure 2a). Their refined features were revealed by SEM image (Figure 2b), which showed uniform depth of threads (about 100 μm) with thread pitch of 600 μm. In addition, the screw displayed relatively homogeneous appearance at scale of few hundreds of microns, while a rougher surface at scale of several microns (Figure S1, supporting information). A high roughness profile at several microns scale should improve early fixation and long-term stability due to the mechanical interlocking between the implants and bone ingrowth [44]. Moreover, this rough topographic features play a decisive role on the biological response to orthopedic implants [45]. We then evaluated the mechanical properties of the obtained silk orthopedic devices. Shear forces are one of the most prominent forces experienced by bone fixation devices. Silk pins with a diameter of 1.5 mm were used to determine the maximum shear stress (Figure 2g). The silk pins reached a maximum shear stress of 80.2 ± 8.5 MPa, which is comparable to that of the HFIP solvent-based systems (~ 90 MPa) [28]. These values are also comparable with the current resorbable systems which have a shear force of 100–185 MPa [46, 47]. The mechanical properties of silk plates were measured by a four-point bending test using four-hole plates of 29 mm length and 2 mm thickness (Figure 2h). The mechanics of aqueous plates (bending stiffness of 206.3 ± 13.8 N/mm, structural stiffness of 18574.4 ±1242.8 N/mm^2, bending strength of 469.6 ± 92.8 N·mm, and bending modulus of 2.7 ± 0.2 GPa) were significantly improved relative to those of solvent-based plates (bending stiffness of 162.8 ± 23.0 N/mm, structural stiffness of 11621.7 ± 2608.7 N/mm^2, bending strength of 389.6 ± 56.4 N·mm, and bending modulus of 1.7 ± 0.3 GPa) [48].

The tight packing of silk nano-globules is a key factor in determining the mechanical properties and machinability of the regenerated silk materials. We explored two alternative processes of fabricating silk blanks (Figure S2, supporting information). Silk blanks obtained by pregelation process can be machined into screws, pins and plates, but the mechanical properties of the devices were significantly lower than those from the biomimetic process. For example, the maximum shear stress of the silk pins was 20.4 ± 1.5

MPa compared to 80.2 ± 8.5 MPa of pins from the biomimetic silk blanks. A close-up view of the surface morphology of the screw revealed a globular structure with nano/micro-sized pores (Figure S3e, supporting information), which corresponds to the pores present in the hydrogel. The less interaction/interlocking between the globules might be responsible for the different mechanical property of the resultant devices. Silk blanks from the fast dehydration process can be machined into pins and plates, but not screws with a more complexed contour. In this process, methanol treatment induced faster formation of fibers/globules with β-sheet structure, resulting in pores and thus more loosely packed structures as revealed by AFM image (Figure S4, supporting information).

We then evaluated the stability of the silk-derived materials in DPBS buffer. After 4-week incubation at 37°C, silk screws maintained their structural integrity and original shape (Figure S5A and B). We also studied the degradation of regenerated silk materials in DPBS and in the presence of proteinase XIV and α-chymotrypsin. As shown in Figure S5D, there was about 10% weight loss when samples were incubated in PBS and α-chymotrypsin after 9 weeks, while there was about 44% weigh loss in protease XIV. The projected *in vitro* degradation time to complete loss of the samples in proteases was approximately 5 months, which is faster than that of HFIP-based silk materials of 7 months [28]. These results are in line with our previous findings that aqueous-derived silk scaffolds degraded faster than HFIP-derived scaffolds *in vivo* [49].

We next evaluated the mechanical properties of the silk-based orthopedic device in the hydrated state. Incorporation of nano-HAP significantly improved the maximum shear force of the silk pins from 80.2 ± 8.5 MPa to 94.1 + 5.7 in the dry state, while from 18.2 ± 1.5 MPa to 23.2 ± 1.2 MPa in the hydrated state (Figure S5D). Although one limitation of the current silk format is the hydrated mechanical strength, adding nHAP reduced swelling and enhanced hydrated mechanics. These findings were consistent with previous studies where the addition of hydroxyapatite reduced the swelling and increased mechanical properties of various types of composite scaffolds [50–52]. Furthermore, the mechanical properties of the silk materials could be improved with the addition of silk micro-fibers or silk micro-particles to meet the mechanical demand for orthopedic use [53,54].

3.3. Osteoinductive silk-based orthopedic devices

One main appeal of the aqueous-based process lies in the development of osteoinductive orthopedic devices. The current metallic and resorbable orthopedic fixation systems do not provide osteogenic functionality. Thanks to the all-aqueous process, silk orthopedic device was functionalized with osteoinductive factors through bulk-incorporation of bone morphogenetic protein 2 (BMP2) or P24 peptide in the fabrication process. P24 is a synthetic BMP-2-related peptide corresponding to residues of the knuckle epitope of BMP-2, which could regulate adhesion and differentiation of bone marrow stromal cells and induce ectopic osteogenesis. Immunostaining of BMP2 demonstrated the uniform incorporation of BMP2 in silk pins. The release kinetics of BMP2 was determined by ELISA and showed a peak release on day1 followed by sustained release over time (Figure S8). The bioactivity of the released BMP2 was verified by improved ALP activity and calcification in stem cells cocultured with BMP2-incorporated silk under osteogenic

conditions (Figure S9, supporting information). A similar low level of BMP2 was reported to improve the gene expression of related osteogenic markers in human osteoblasts [55].

We next generated an *in vitro* cell culture system to mimic the screw-bone interface *in vivo* (Figure 3a). hMSCs were seeded in the porous silk scaffold and cultured under osteogenic conditions for 6 weeks. hMSCs underwent osteogenic differentiation and the resulting mineralization was demonstrated by the positive staining of HAP with OsteoImage. OsteoImage stain was detected at the screw/sponge interface and inside the sponge in BMP2-and P24-incorporated silk screw groups (Figure 3e–j). In contrast, mineralization only occurred at the periphery of the silk sponge in the osteogenic control without BMP2 or P24 (Figure 3b–d). Notably, the deposition of mineralized tissue followed the contour of the screw and was observed in direct contact with the screw surface in the presence of BMP2, which might imply the good osteointegeration of the screw with the bony tissue when implanted *in vivo*. The ability to stabilize and control the release of osteoinductive compound from silk could modulate the concentrations to local microenvironments, avoiding ectopic bone complications and optimizing sustained functional features as needed. This control would offer a distinct advantage of not only being biodegradable and resorbable but actually promoting and inducing bone growth and remodeling only locally.

3.4. Antimicrobial and biocomposite silk-based orthopedic device

Another advantage of the biomimetic fabrication process is to add antimicrobial functionality to the system. Incorporation of antibiotics within biodegradable orthopedic implants could provide an approach for local antimicrobial prophylaxis of biomaterial-related infections without significant systematic exposure. This is a major need for orthopedic repairs [56]. For this purpose, silk devices containing ciprofloxacin were prepared (Figure 4a). Ciprofloxacin was selected in this study as it possesses a broad spectrum of activity, including most osteomyelitis-causing pathogens, such as *S. aureus*. The antimicrobial effect of the silk/ciprofloxacin pins was demonstrated by a zone of inhibition assay, and a clear zone lacking bacteria growth formed around the ciprofloxacin-containing silk rods placed on the *S. aureus* bacterial lawn (Figure 4b). We then evaluated biofilm formation on ciprofloxacin-loaded silk pins using *S. epidermidis*. *S. epidermidis* is one of the leading etiologic agents associated with orthopedic implant-related infections, and it can adhere to and aggregate on biomaterials surface and can form biofilms on many biomaterials [57]. The biofilm formation was completely inhibited on ciprofloxacin-loaded pins, whereas biofilm patches were observed on silk pins without antibiotics (Fig. 4c and d).

The release of ciprofloxacin was carried out in PBS as well as in the presence of protease IXV to model the potential *in vivo* proteolytic degradation of the silk. The continuous release of ciprofloxacin was sustained for at least 36 days, suggesting that the bioactivity of the sensitive therapeutics was preserved during the mild, aqueous processing fabrication process. This stabilization effect of silk on antibiotic activity was consistent with previous findings on antibiotics stabilization within silk materials of various formats [58, 59]. In addition, ciprofloxacin release in protease solution was significantly faster than that in PBS, which suggested that the release profile can be tuned by silk degradation. Therefore, the

ciprofloxacin-releasing orthopedic devices represent a novel system for long term delivery of antibiotics to prevent orthopedic-related infections.

One major objective of current orthopedic repair strategies is to enhance the microenvironment of metallic implants by enhancing osteoconduction. Composite screws have previously been developed by the addition of inorganic fillers such as HAP and β-tricalcium phosphate due to their proven osteoconductivity [60, 61]. Studies have also shown that silica-containing materials, such as silica nanoparticle, could stimulate the differentiation and activity of bone-building osteoblast but suppress bone-resorbing osteoclast *in vitro* [62,63]. In this study, we incorporated HAP and silica nanoparticles in silk blanks and successfully machined the resulting composite blanks into orthopedic devices. The composite materials showed similar machinability to silk alone. For example, silk/HAP and silk/SiO_2 biocomposite screws showed a smooth surface finish after machining (Figure 4f, g, i and j). The FTIR analysis revealed the presence of HAP and silica nanoparticles in the screw (Figure 4h and k). Silk proteins, including silk fibroin and sericin, have been used as biotemplates for the formation of inorganic/organic composite materials with controlled morphology, organization and hierarchies with the aim of enhancing properties [64–67]. For example, silk and silk sericin were selected as substitutes for collagen I to synthesize HAP composite materials for potential utilization in bone tissue engineering [64, 66]. The incorporation of HAP improved cell attachment, proliferation, and most importantly, enhanced the osteogenic differentiation of bone marrow derived stem cells [66]. Thus, this new class of biocomposite orthopedic devices has the potential of providing improved bioactivity and better osteointegration with surrounding bone tissue.

4. Conclusions

In summary, we demonstrated the feasibility of generating machinable silk materials *via* a biomimetic, all-aqueous process. We focused on the dehydration of silk solutions and the assembly of silk molecules to generate compact crystalline structures, as a route to generate highly dense, organized building blocks from which to generate mechanically robust silk-based orthopedic devices. The mild, all-aqueous process provides a wide range of opportunities by combining silk with other biomolecules (e.g., antibiotics, growth factors, cytokines), thus providing useful avenues for functionalized orthopedic devices.

Supplementary Material

Refer to Web version on PubMed Central for supplementary material.

Acknowledgments

We thank the NIH (R01 AR068048) for support of this study.

References

1. Magoshi, J.; Magoshi, Y.; Becker, MA.; Nakamura, S. Polymeric materials encyclopedia. Salamone, JC., editor. CRC Press; Boca Raton, FL: 1996. p. 667-679.
2. Jin HJ, Kaplan DL. Mechanism of silk processing in insects and spiders. Nature. 2003; 424(6952): 1057–1061. [PubMed: 12944968]

3. Luo J, Zhang L, Peng Q, Sun M, Zhang Y, Shao H, Hu X. Tough silk fibers prepared in air using a biomimetic microfluidic chip. Int J Biol Macromol. 2014; 66:319–324. [PubMed: 24613677]
4. Sun M, Zhang Y, Zhao Y, Shao H, Hu X. The structure-property relationships of artificial silk fabricated by dry-spinning process. J Mater Chem. 2012; 22(35):18372–18379.
5. Zhou G, Shao Z, Knight DP, Yan J, Chen X. Silk Fibers Extruded Artificially from Aqueous Solutions of Regenerated Bombyx mori Silk Fibroin are Tougher than their Natural Counterparts. Adv Mater. 2009; 21(3):366–370.
6. Goldberg DS, Bartlett SP, Yu JC, Hunter JV, Whitaker LA. Critical review of microfixation in pediatric craniofacial surgery. J Craniofac Surg. 1995; 6(4):301–307. [PubMed: 9020705]
7. Zhang J, Ebraheim N, Lausé GE, Xiao B, Xu R. A comparison of absorbable screws and metallic plates in treating calcaneal fractures: A prospective randomized trial. J Trauma Acute Care Surg. 2012; 72(2):E106–E110. [PubMed: 22439244]
8. Eglin D, Alini M. Degradable polymeric materials for osteosynthesis: tutorial. Eur Cells & Mat. 2008; 16:80–91.
9. Goodman SB, Yao Z, Keeney M, Yang F. The future of biologic coatings for orthopaedic implants. Biomaterials. 2013; 34(13):3174–3183. [PubMed: 23391496]
10. Chambers B, St Clair SF, Froimson MI. Hydroxyapatite-Coated Tapered Cementless Femoral Components in Total Hip Arthroplasty. J Arthroplasty. 2007; 22(4, Supplement):71–74.
11. Choi S, Murphy WL. Sustained plasmid DNA release from dissolving mineral coatings. Acta Biomaterialia. 2010; 6(9):3426–3435. [PubMed: 20304109]
12. Reikerås O, Gunderson RB. Excellent results of HA coating on a grit-blasted stem: 245 patients followed for 8–12 years. Acta Orthop Scand. 2003; 74(2):140–145. [PubMed: 12807319]
13. Shah NJ, Hong J, Hyder MN, Hammond PT. Osteophilic Multilayer Coatings for Accelerated Bone Tissue Growth. Adv Mat. 2012; 24(11):1445–1450.
14. Rammelt S, Illert T, Bierbaum S, Scharnweber D, Zwipp H, Schneiders W. Coating of titanium implants with collagen, RGD peptide and chondroitin sulfate. Biomaterials. 2006; 27(32):5561–5571. [PubMed: 16879866]
15. Macdonald ML, Samuel RE, Shah NJ, Padera RF, Beben YM, Hammond PT. Tissue integration of growth factor-eluting layer-by-layer polyelectrolyte multilayer coated implants. Biomaterials. 2011; 32(5):1446–1453. [PubMed: 21084117]
16. Crouzier T, Ren K, Nicolas C, Roy C, Picart C. Layer-By-Layer Films as a Biomimetic Reservoir for rhBMP-2 Delivery: Controlled Differentiation of Myoblasts to Osteoblasts. Small. 2009; 5(5):598–608. [PubMed: 19219837]
17. Liu Y, de Groot K, Hunziker EB. BMP-2 liberated from biomimetic implant coatings induces and sustains direct ossification in an ectopic rat model. Bone. 2005; 36(5):745–757. [PubMed: 15814303]
18. Elmengaard B, Bechtold JE, Søballe K. In vivo study of the effect of RGD treatment on bone ongrowth on press-fit titanium alloy implants. Biomaterials. 2005; 26(17):3521–3526. [PubMed: 15621242]
19. Peter B, Pioletti DP, Laïb S, Bujoli B, Pilet P, Janvier P, Guicheux J, Zambelli PY, Bouler JM, Gauthier O. Calcium phosphate drug delivery system: influence of local zoledronate release on bone implant osteointegration. Bone. 2005; 36(1):52–60. [PubMed: 15664002]
20. Tengvall P, Skoglund B, Askendal A, Aspenberg P. Surface immobilized bisphosphonate improves stainless-steel screw fixation in rats. Biomaterials. 2004; 25(11):2133–2138. [PubMed: 14741628]
21. Tanzer M, Karabasz D, Krygier JJC, Cohen R, Bobyn JD. THE OTTO AUFRANC AWARD: Bone Augmentation around and within Porous Implants by Local Bisphosphonate Elution. Clin Orthop Relat Res. 2005:30–39.
22. Zhang F, Zhang Z, Zhu X, Kang ET, Neoh KG. Silk-functionalized titanium surfaces for enhancing osteoblast functions and reducing bacterial adhesion. Biomaterials. 2008; 29(36):4751–4759. [PubMed: 18829101]
23. Kingshott P, Wei J, Bagge-Ravn D, Gadegaard N, Gram L. Covalent Attachment of Poly(ethylene glycol) to Surfaces, Critical for Reducing Bacterial Adhesion. Langmuir. 2003; 19(17):6912–6921.
24. Rodrigues L, Banat IM, Teixeira J, Oliveira R. Biosurfactants: potential applications in medicine. J Antimicrob Chemother. 2006; 57(4):609–618. [PubMed: 16469849]

25. Guillaume O, Garric X, Lavigne JP, Van Den Berghe H, Coudane J. Multilayer, degradable coating as a carrier for the sustained release of antibiotics: Preparation and antimicrobial efficacy in vitro. J Control Release. 2012; 162(3):492–501. [PubMed: 22902589]
26. Radin S, Ducheyne P. Controlled release of vancomycin from thin sol–gel films on titanium alloy fracture plate material. Biomaterials. 2007; 28(9):1721–1729. [PubMed: 17184835]
27. Zhang W, Luo Y, Wang H, Jiang J, Pu S, Chu PK. Ag and Ag/N2 plasma modification of polyethylene for the enhancement of antibacterial properties and cell growth/proliferation. Acta Biomaterialia. 2008; 4(6):2028–2036. [PubMed: 18586586]
28. Chen W, Liu Y, Courtney HS, Bettenga M, Agrawal CM, Bumgardner JD, Ong JL. In vitro anti-bacterial and biological properties of magnetron co-sputtered silver-containing hydroxyapatite coating. Biomaterials. 2006; 27(32):5512–5517. [PubMed: 16872671]
29. Perrone GS, Leisk GG, Lo TJ, Moreau JE, Haas DS, Papenburg BJ, Golden EB, Partlow BP, Fox SE, Ibrahim AMS, Lin SJ, Kaplan DL. The use of silk-based devices for fracture fixation. Nat Commun. 2014; 5
30. Vepari C, Kaplan DL. Silk as a biomaterial. Prog Polym Sci. 2007; 32(8–9):991–1007. [PubMed: 19543442]
31. Li AB, Kluge JA, Guziewicz NA, Omenetto FG, Kaplan DL. Silk-based stabilization of biomacromolecules. J Control Release. 2015; 219:416–430. [PubMed: 26403801]
32. Rockwood DN, Preda RC, Yucel T, Wang X, Lovett ML, Kaplan DL. Materials fabrication from Bombyx mori silk fibroin. Nat Protoc. 2011; 6(10):1612–1631. [PubMed: 21959241]
33. Mujika F. On the difference between flexural moduli obtained by three-point and four-point bending tests. Polym Test. 2006; 25(2):214–220.
34. Wegst UGK, Bai H, Saiz E, Tomsia AP, Ritchie RO. Bioinspired structural materials. Nature Mater. 2015; 14(1):23–36. [PubMed: 25344782]
35. Pérez-Rigueiro J, Elices M, Plaza GR, Guinea GV. Similarities and Differences in the Supramolecular Organization of Silkworm and Spider Silk. Macromolecules. 2007; 40(15):5360–5365.
36. Reinstädler D, Fabian H, Naumann D. New structural insights into the refolding of ribonuclease T1 as seen by time-resolved Fourier-transform infrared spectroscopy. Proteins: Struct Funct Bioinform. 1999; 34(3):303–316.
37. Barth A. The infrared absorption of amino acid side chains. Prog Biophys Mol Biol. 2000; 74(3–5):141–173. [PubMed: 11226511]
38. Hu X, Kaplan D, Cebe P. Determining Beta-Sheet Crystallinity in Fibrous Proteins by Thermal Analysis and Infrared Spectroscopy. Macromolecules. 2006; 39(18):6161–6170.
39. Saluja A, Kalonia DS. Nature and consequences of protein–protein interactions in high protein concentration solutions. Int J Pharm. 2008; 358(1–2):1–15. [PubMed: 18485634]
40. Stradner A, Sedgwick H, Cardinaux F, Poon WCK, Egelhaaf SU, Schurtenberger P. Equilibrium cluster formation in concentrated protein solutions and colloids. Nature. 2004; 432(7016):492–495. [PubMed: 15565151]
41. Yearley, Eric J.; Godfrin, Paul D.; Perevozchikova, T.; Zhang, H.; Falus, P.; Porcar, L.; Nagao, M.; Curtis, Joseph E.; Gawande, P.; Taing, R.; Zarraga, Isidro E.; Wagner, Norman J.; Liu, Y. Observation of Small Cluster Formation in Concentrated Monoclonal Antibody Solutions and Its Implications to Solution Viscosity. Biophys J. 2014; 106(8):1763–1770. [PubMed: 24739175]
42. Brown CP, Harnagea C, Gill HS, Price AJ, Traversa E, Licoccia S, Rosei F. Rough Fibrils Provide a Toughening Mechanism in Biological Fibers. ACS Nano. 2012; 6(3):1961–1969. [PubMed: 22324287]
43. Henkel J, Woodruff MA, Epari DR, Steck R, Glatt V, Dickinson IC, Choong PFM, Schuetz MA, Hutmacher DW. Bone Regeneration Based on Tissue Engineering Conceptions — A 21st Century Perspective. Bone Res. 2013; 1:216–248. [PubMed: 26273505]
44. Shalabi MM, Gortemaker A, Hof MAVt, Jansen JA, Creugers NHJ. Implant Surface Roughness and Bone Healing: a Systematic Review. J Dent Res. 2006; 85(6):496–500. [PubMed: 16723643]
45. Jager M, Zilkens C, Zanger K, Krauspe R. Significance of Nano- and Microtopography for Cell-Surface Interactions in Orthopaedic Implants. J Biomed Biotechnol. 2007; 2007:96036.

46. Ashammakhi N, Veiranto M, Suokas E, Tiainen J, Niemelä SM, Törmälä P. Innovation in multifunctional bioabsorbable osteoconductive drug-releasing hard tissue fixation devices. J Mater Sci Mater Med. 2006; 17(12):1275–1282. [PubMed: 17143759]
47. Leinonen S, Suokas E, Veiranto M, Törmälä P, Waris T, Ashammakhi N. Holding Power of Bioabsorbable Ciprofloxacin-Containing Self-reinforced Poly-L/DL-lactide 70/30 Bioactive Glass 13 Miniscrews in Human Cadaver Bone. J Craniofac Surg. 2002; 13(2):212–218. [PubMed: 12000875]
48. Haas, DS. Biomed Eng. Tufts University; Boston, MA: 2015. Design and Optimization of Resorbable Silk Internal Fixation Devices; p. 128
49. Wang Y, Rudym DD, Walsh A, Abrahamsen L, Kim HJ, Kim HS, Kirker-Head C, Kaplan DL. In vivo degradation of three-dimensional silk fibroin scaffolds. Biomaterials. 2008; 29(24–25):3415–3428. [PubMed: 18502501]
50. Peter M, Ganesh N, Selvamurugan N, Nair SV, Furuike T, Tamura H, Jayakumar R. Preparation and characterization of chitosan–gelatin/nanohydroxyapatite composite scaffolds for tissue engineering applications. Carbohydr Polym. 2010; 80(3):687–694.
51. Reves BT, Jennings JA, Bumgardner JD, Haggard WO. Preparation and Functional Assessment of Composite Chitosan-Nano-Hydroxyapatite Scaffolds for Bone Regeneration. J Func Biomater. 2012; 3(1):114–130.
52. Thein-Han WW, Misra RD. Biomimetic chitosan-nanohydroxyapatite composite scaffolds for bone tissue engineering. Acta Biomater. 2009; 5(4):1182–97. [PubMed: 19121983]
53. Mandal BB, Grinberg A, Seok Gil E, Panilaitis B, Kaplan DL. High-strength silk protein scaffolds for bone repair. Proceedings of the National Academy of Sciences. 2012; 109(20):7699–7704.
54. Rajkhowa R, Gil ES, Kluge J, Numata K, Wang L, Wang X, Kaplan DL. Reinforcing Silk Scaffolds with Silk Particles. Macromol Biosci. 2010; 10(6):599–611. [PubMed: 20166230]
55. Draenert FG, Nonnenmacher AL, Kammerer PW, Goldschmitt J, Wagner W. BMP-2 and bFGF release and in vitro effect on human osteoblasts after adsorption to bone grafts and biomaterials. Clin Oral Implants Res. 2013; 24(7):750–7. [PubMed: 22524399]
56. Mäkinen TJ, Veiranto M, Knuuti J, Jalava J, Törmälä P, Aro HT. Efficacy of bioabsorbable antibiotic containing bone screw in the prevention of biomaterial-related infection due to Staphylococcus aureus. Bone. 2005; 36(2):292–299. [PubMed: 15780955]
57. Montanaro L, Speziale P, Campoccia D, Ravaioli S, Cangini I, Pietrocola G, Giannini S, Arciola CR. Scenery of Staphylococcus implant infections in orthopedics. Future Microbiol. 2011; 6(11): 1329–1349. [PubMed: 22082292]
58. Pritchard EM, Valentin T, Panilaitis B, Omenetto F, Kaplan DL. Antibiotic-Releasing Silk Biomaterials for Infection Prevention and Treatment. Adv Funct Mater. 2013; 23(7):854–861. [PubMed: 23483738]
59. Zhang J, Pritchard E, Hu X, Valentin T, Panilaitis B, Omenetto FG, Kaplan DL. Stabilization of vaccines and antibiotics in silk and eliminating the cold chain. Proc Natl Acad Sci USA. 2012; 109(30):11981–11986. [PubMed: 22778443]
60. Arthrex Research and Development. Arthrex BioComposite Interference Screws for ACL and PCL Reconstruction. 2010
61. Johnston M, Morse A, Arrington J, Pliner M, Gasser S. Resorption and Remodeling of Hydroxyapatite–Poly-L-Lactic Acid Composite Anterior Cruciate Ligament Interference Screws. Arthroscopy. 2011; 27(12):1671–1678. [PubMed: 21978431]
62. Ha SW, Weitzmann MN, Beck GR. Bioactive Silica Nanoparticles Promote Osteoblast Differentiation through Stimulation of Autophagy and Direct Association with LC3 and p62. ACS Nano. 2014; 8(6):5898–5910. [PubMed: 24806912]
63. Jiao K, Niu L-n, Li Q-h, Chen F-m, Zhao W, Li J-j, Chen J-h, Cutler CW, Pashley DH, Tay FR. Biphasic silica/apatite co-mineralized collagen scaffolds stimulate osteogenesis and inhibit RANKL-mediated osteoclastogenesis. Acta Biomater. 2015; 19:23–32. [PubMed: 25792280]
64. Cai Y, Yao J. Effect of proteins on the synthesis and assembly of calcium phosphate nanomaterials. Nanoscale. 2010; 2(10):1842–1848. [PubMed: 20676452]

65. Fei X, Li W, Shao Z, Seeger S, Zhao D, Chen X. Protein Biomineralized Nanoporous Inorganic Mesocrystals with Tunable Hierarchical Nanostructures. J Am Chem Soc. 2014; 136(44):15781–15786. [PubMed: 25325188]

66. Yang M, Shuai Y, Zhang C, Chen Y, Zhu L, Mao C, OuYang H. Biomimetic nucleation of hydroxyapatite crystals mediated by Antheraea pernyi silk sericin promotes osteogenic differentiation of human bone marrow derived mesenchymal stem cells. Biomacromolecules. 2014; 15(4):1185–93. [PubMed: 24666022]

67. Yang M, Shuai Y, Zhou G, Mandal N, Zhu L, Mao C. Tuning Molecular Weights of Bombyx mori (B. mori) Silk Sericin to Modify Its Assembly Structures and Materials Formation. ACS Appl Mater Interfaces. 2014; 6(16):13782–13789. [PubMed: 25050697]

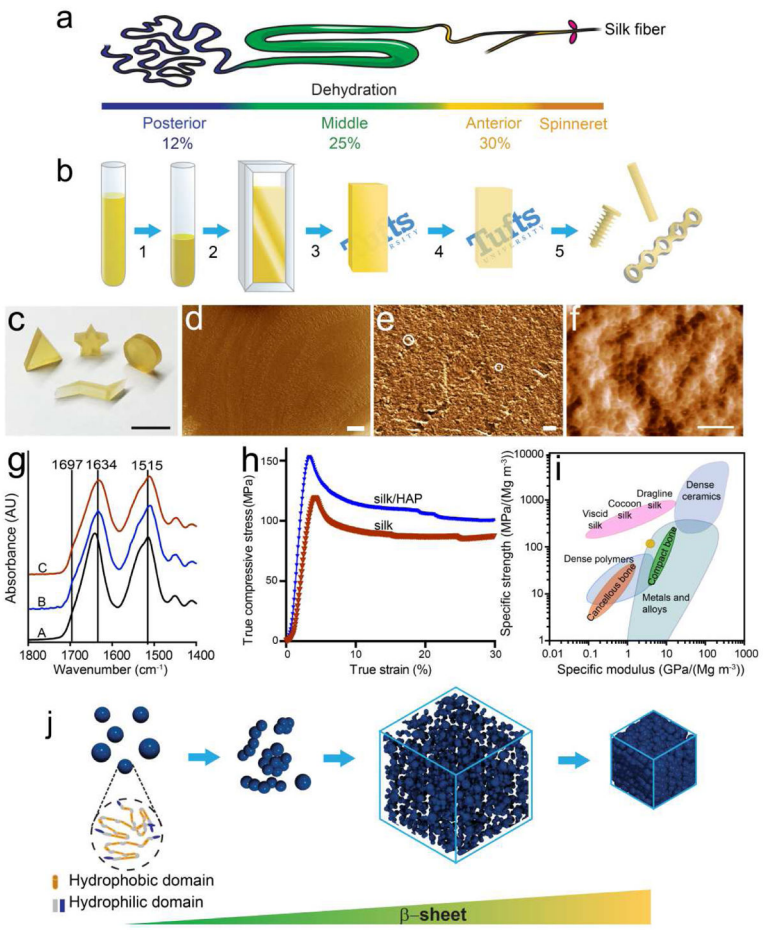

Figure 1.

Schematic illustration of the fabrication process, characterization and assembly mechanism of biomimetic silk materials. (a) Illustration of spinning duct of silkworm. (b) Solid silk materials were obtained by the biomimetic gradual dehydration of silk aqueous solution. (1) Concentrate silk solution to 25–30% (wt/wt). (2) Inject concentrated silk solution to silk blank molds. (3) Remove water by forced air flow at 10°C for 3–4 days. (4) Remove the remaining water by drying in fume hood at room temperature for 4 days and then in an oven at 45°C for 4 days. (5) Machine silk blank into orthopedic devices of desired geometry. (c) Various shapes machined from biomimetic silk materials (scale = 1 cm). (d, e) SEM and (f) AFM images of the cross section of a silk rod of 1.5 mm diameter (scale: 40 μm in d, 2 μm in e, and 200 nm in f.). (g) FTIR spectra of silk materials (A: freeze-dried concentrated silk solution; B: silk materials obtained after dehydration at 10°C and room temperature; C: silk blanks before machining.) (h) Stress-strain curve of biomimetic silk materials. (i) Comparison of specific strength and modulus of the biomimetic silk material with natural silk materials, bone, polymer, ceramic and metal/alloys. Adapted with permission from nature publishing group [34]. The yellow ellipse represents the silk and silk/HAP materials in this study. (j) Model of the assembly process of the biomimetic silk materials. The silk molecules form oligomeric aggregates in concentrated silk solution. Dehydration leads to the condensation and assembly of the silk molecules into densely packed solid materials.

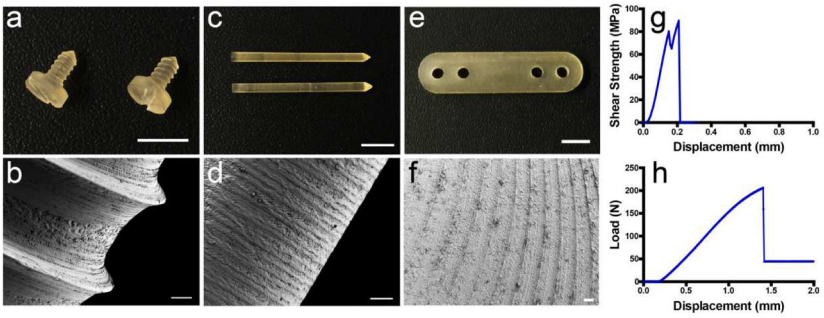

Figure 2.

Silk orthopedic devices. (a) Silk screw with bone screw thread. Scale = 5 mm. The major diameter of the screw was ~ 1.8 mm and pitch was 600 μm. (b) SEM image of bone screw (scale = 100 μm). (c) Silk IM rods of 1.5 mm diameter, scale = 5 mm. (d) SEM image of silk IM rods, scale = 5 mm. (e) Four-hole silk plate of 29 mm length and 2 mm thickness (scale = 5 mm). (f) SEM image of milled surface of silk plate (scale = 100 μm). (g) Representative shear strength-displacement curve of 1.5 mm diameter silk pin by double lap shear mechanical test. (h) Representative load-displacement curve of the four-hole silk plate of 29 mm length and 2 mm thickness by four-point bending test.

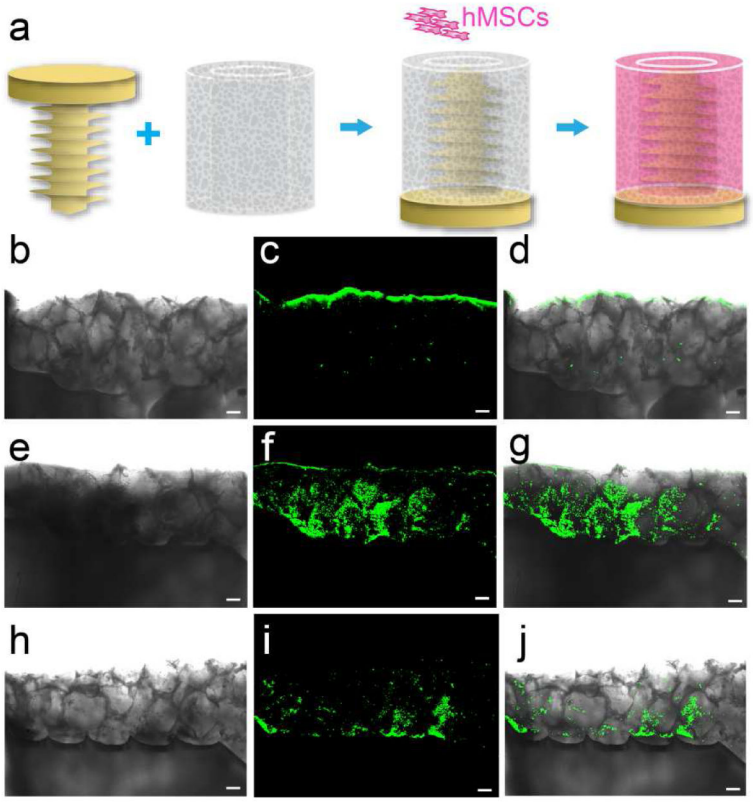

Figure 3.

Silk-based orthopedic devices with osteoinductive functionality: *in vitro* differentiation of hMSCs induced by BMP2/P24 incorporated silk screws. (a) Schematic illustrating the *in vitro* cell culture setup. BMP2/P24 incorporated silk screws were inserted into a tubular silk sponge with pore size of 400–500 μm and hMSCs were seeded in the sponge. Osteogenic differentiation of hMSCs was assessed with OsteoImage fluorescent staining for HAP after 6-week culture in osteogenic medium. Transmitted light (b, e and h), fluorescent (c, f and i) and overlay images demonstrated the mineralization pattern in (b–d) osteogenic control, (e–g) BMP2 and (h–j) P24 groups. Scale = 200 μm.

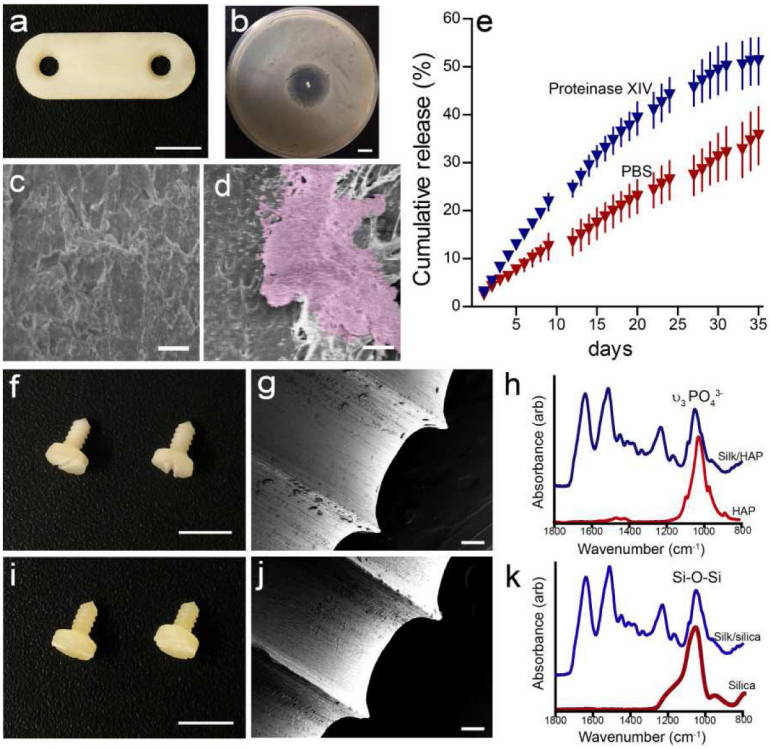

Figure 4.

Silk-based antimicrobial and biocomposite orthopedic devices. (a) Two-hole plate containing 5% (wt/wt) ciprofloxacin (scale = 5 mm). (b) A clear zone of inhibition formed around ciprofloxacin releasing silk rods against *S. aureus* cultures (scale = 1mm). SEM of biofilm on (c) ciprofloxacin-loaded and (d) pure silk pins, scale = 10 μm. (e) The cumulative release of ciprofloxacin from ciprofloxacin-loaded silk rod over 36 days. (f and i) Optical images, (g and j) SEM images and (h and k) FTIR spectra of the (f–h) silk/HAP (90/10 wt/wt) and (i–k) silk/SiO_2 (90/10 wt/wt) biocomposite screw with bone screw thread. Scale = 5 mm in d and g and 100 μm in e and h, respectively.